Electronic Supplementary Material (ESI) for Nanoscale Horizons.

Prediction of Room-Temperature Ferromagnetism and Large Perpendicular Magnetic Anisotropy in a Planar Hypercoordinate FeB_3 Monolayer

Cheng Tang[1,2], Kostya (Ken) Ostrikov[1,2], Stefano Sanvito[3], Aijun Du[1,2,]*

[1]Centre for Materials Science, Queensland University of Technology, Brisbane, QLD 4000, Australia

[2]School of Chemistry and Physics, Queensland University of Technology, Brisbane, QLD 4000, Australia

Email: aijun.du@qut.edu.au

[3]School of Physics and CRANN Institute, Trinity College, Dublin 2, Ireland

Computational Details

The phonon spectrum was obtained by phonopy code with the finite difference method [1], and Curie (Néel) temperature was simulated by Monte Carlo method in Vampire package [2]. The Monte Carlo steps were set to be 1×10^5 followed by 1.5×10^5 steps for time averaging at each temperature. The simulated geometry is taken to be 15×15 nm for both of the structures [3]. By using such parameters, the estimated transition temperature of CrI_3 is 46 K, almost the same as the experimental results, suggesting the reliability of our simulations. The thermal stability was examined by *Ab initio* molecular dynamic (AIMD) simulation within a large 5×5×1 supercell for α-FeB_3 for 10 ps with a time step of 1 fs. The different supercell is adopted to fulfill the requirement of even iron atoms for AFM configuration. The Nosé-Hoover chains were used to control the temperature [4]. Moreover, the structural search of 2D FeB_3 was performed by the CALYPSO code [5, 6] with the population size being set to 30. Thus, 900 predicted structures were calculated for each stoichiometry during the simulation, in which 60 % of them were evolved into next generation by particle swarm optimization (PSO), while others were randomly generated.

Besides, the cohesive energies, E_{coh}, is defined by

$$E_{coh} = (xE_{Fe} + 3xE_B - xE_{FeB3})/4x$$

where E_{Fe}, E_B and E_{FeB3} are the total energies of a single iron, a single boron and the unit cell of FeB_3 monolayer, respectively.

The magnetic-exchange parameters, *J*, can be computed through the Heisenberg spin Hamiltonian

$$H = -\sum_i J_i(R) \sum_{<mn>} \vec{S}_m \vec{S}_n + \sum_m K_m (\vec{S}_m^z \vec{A}_m)^2$$

where i represents the i-th nearest neighbouring magnetic couplings. $\vec{S}$ is the magnetic moment of Fe atoms, while K and $\vec{A}$ represent the coefficient of anisotropy and magnetocrystalline axis.

The mechanical performance is explored by the in-plane Young's modulus Y(θ) and Poisson's ratio ν(θ) as follows

$$Y(\theta) = \frac{C_{11}C_{22} - C_{12}^2}{C_{11}s^4 + C_{22}c^4 + As^2c^2}$$

$$\nu(\theta) = -\frac{Bc^2s^2 - C_{12}(c^4 + s^4)}{C_{11}s^4 + C_{22}c^4 + As^2c^2}$$

where $s = sin\theta, c = cos\theta, A = (C_{11}C_{22} - C_{12}^2)/C_{66} - 2C_{12}$ and $B = C_{11} + C_{22} - (C_{11}C_{22} - C_{12}^2)/C_{66}$.

The Fermi velocity is defined as $v_F = \frac{1}{h}\partial E/\partial k$, where *h* is the Planck's constant and ($\partial E/\partial k$) is the slope of band structures near Dirac points in the reciprocal space.

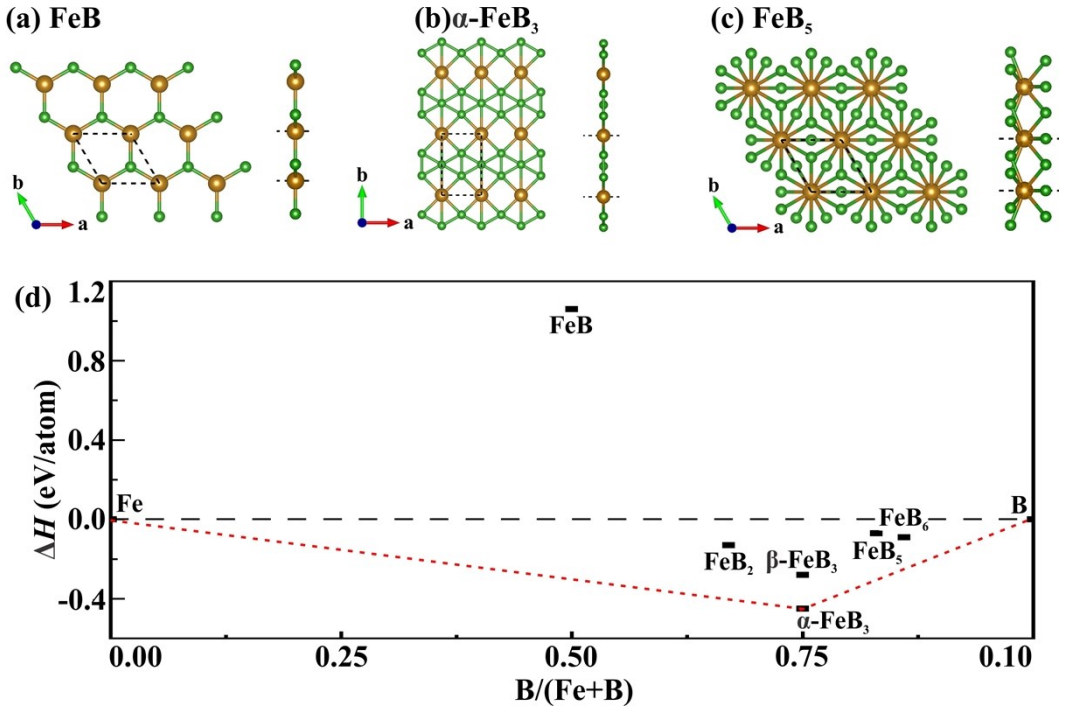

Fig. S1. (a, b, c) The top and side views of the predicted FeB_{2x+1} monolayers with the lowest energy in each composition. The dark yellow and green balls represent the iron and boron atoms, respectively. (d) Convex Hull data for FeB_n monolayers with respect to the most stable phase of Fe and Borophene. The previously predicted stable geometries of FeB_2 and FeB_4 monolayers [7, 8] are used as the references to check the stability of our newly predicted FeB_{2n+1} monolayers. The results indicate that our predicted α-FeB_3 monolayer is more thermodynamically stable than other discovered allotropes.

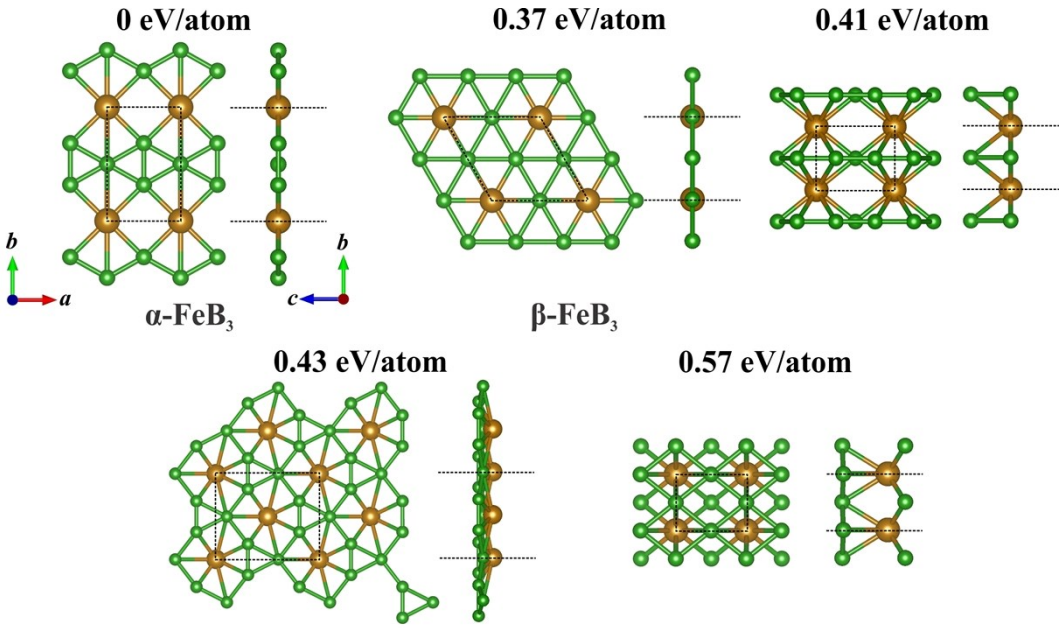

Fig. S2. The top and side views of predicted FeB_3 monolayers with lower energy by CALYPSO code. The relative energy with respect to the most stable one is calculated by the GGA+U method.

Mechanical Properties

In order to investigate the lattice distortions of α-FeB_3 monolayer, we calculated the Young's modulus (Y) and Poisson's ratio (ν) as a function of the in-plane angle (θ) based on the obtained elastic constants. As shown in Fig. S3, the Young's modulus are 175.04 and 128.17 N/m along the *a* and *b* direction, respectively, indicating the anisotropic distortions under external strains. This also reflects the interactions between B-B bond in B framework (the *a* direction) is much stronger than that of Fe-B bonds along the *b* direction. Besides, the Poisson's Ratio of α-FeB_3 reaches 0.67 in some direction, due to its compressible and anisotropic distortion in some directions.

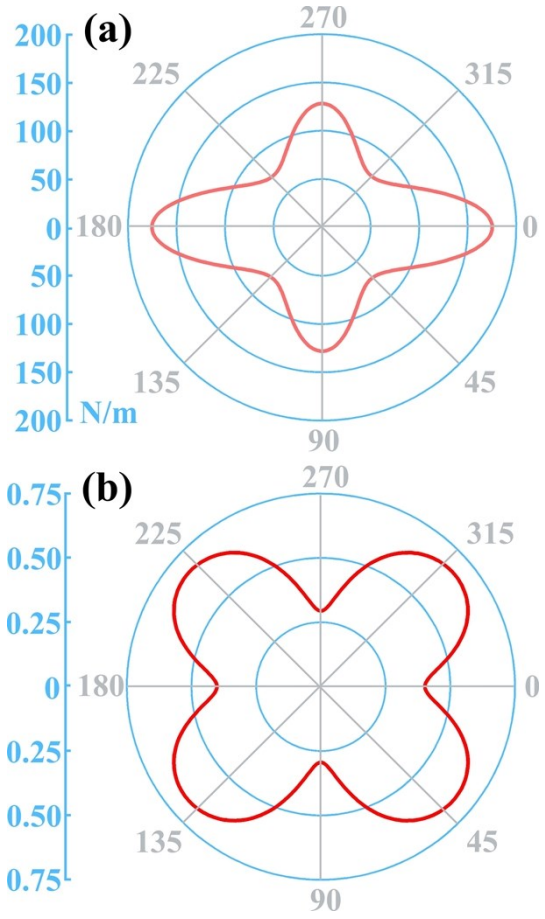

Fig. S3. Polar diagrams of (a) Young's modulus and (b) Poisson's ratio for α-FeB_3.

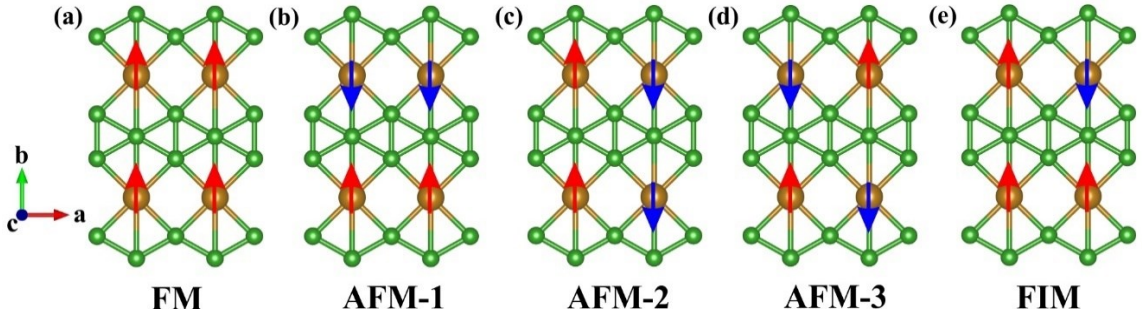

Fig. S4. The magnetic configurations of (a) ferromagnetism (FM), (b-d) antiferromagnetism (AFM) and (e) ferrimagnetism (FIM) for α-FeB_3 monolayer.

Table S1. Total energies (eV) of α-FeB_3 monolayer under different magnetic configurations. (The spin state is along the out-of-plane direction in SOC calculations.)

Configurations	FM	AFM-1	AFM-2	AFM-3	FIM	NM
GGA+U	**-97.74705**	-96.04374	-96.89916	-96.51346	-97.46528	-90.73237
GGA+U+SOC	**-97.78406**	-97.39183	-97.59994	-97.53765	-97.50519	-

Magnetic coupling parameters calculation

Based on the Heisenberg model, the energies (E) for different magnetic configurations in a 2×2 supercell are shown as following,

$E_{FM} = E_0 - (4J_1 + 4J_2 + 8J_3)|\vec{S}|^2$

$E_{AFM-1} = E_0 - (4J_1 - 4J_2 - 8J_3)|\vec{S}|^2$

$E_{AFM-2} = E_0 - (-4J_1 + 4J_2 - 8J_3)|\vec{S}|^2$

$E_{AFM-3} = E_0 - (-4J_1 - 4J_2 + 8J_3)|\vec{S}|^2$

where $|\vec{S}|$ is the value of magnetic moment of Fe atoms in α-FeB_3, it is $\frac{3}{2}\mu_B$ in our calculation. Then, we can estimate the magnetic coupling parameters (J_1, J_2 and J_3) by solving the above equations.

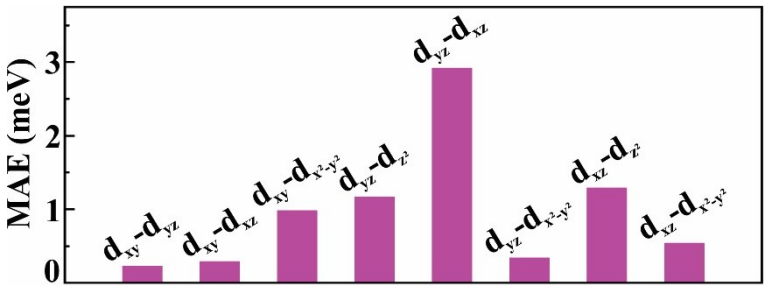

Fig. S5. The orbital resolved magnetic anisotropic energy with respect to the d orbital couplings.

Table S2. The calculated total energies (eV) for strained α-FeB_3 monolayer (-5%~5%) under different magnetic configurations.

	FM	AFM-1	AFM-2	AFM-3
-5%	-89.436719	**-93.040652**	-89.057471	-88.618913
-4%	-92.751146	**-94.015608**	-92.192178	-92.038464
-3%	**-95.092142**	-94.971706	-94.419638	-94.48516
-2%	**-96.840374**	-95.841597	-95.660991	-96.201448
-1%	**-97.496412**	-96.193225	-96.571402	-96.359406
0%	**-97.747053**	-96.04374	-96.899164	-96.513455
1%	**-97.180754**	-95.185383	-96.582267	-96.012705
2%	**-96.661371**	-94.880234	-96.0992535	-95.582034
3%	**-94.869349**	-93.729039	-94.853421	-94.445502
4%	-92.940882	-92.146352	**-93.124783**	-92.889479
5%	-91.176935	-91.935266	**-92.854392**	-91.215071

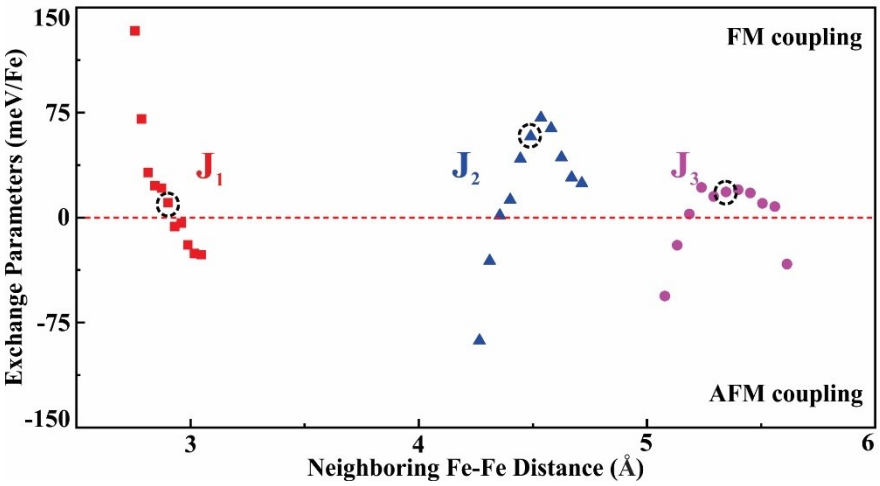

Fig. S6. The calculated exchange parameters of α-FeB_3 monolayer under different biaxial strains. J_1, J_2 and J_3 are the exchange parameters between the nearest, second-nearest and third-nearest neighboring Fe atoms. The circled parameters are for the unstrained monolayer.

Table S3. Total energies (eV) for charge carrier doped α-FeB_3 monolayer under different magnetic configurations.

	FM	AFM-1	AFM-2	AFM-3
0.5h	**-84.091700**	-83.901562	-83.834539	-82.990169
0.4h	**-88.104309**	-87.264437	-87.467172	-86.892144
0.3h	**-91.498777**	-89.962608	-90.724591	-90.204562
0.2h	**-94.59247**	-92.58021	-93.38704	-92.915977
0.1h	**-96.357847**	-94.592119	-95.454791	-95.017821
0	**-97.747053**	-96.04374	-96.899164	-96.513455
0.1e	**-98.566512**	-97.714878	-97.818354	-97.410151
0.2e	**-98.920398**	-98.096186	-98.209425	-97.799036
0.3e	**-99.299625**	-98.478724	-98.608669	-98.183182
0.4e	**-99.687582**	-98.894261	-99.017024	-98.579688
0.5e	**-100.06792**	-99.313577	-99.419081	-98.969319

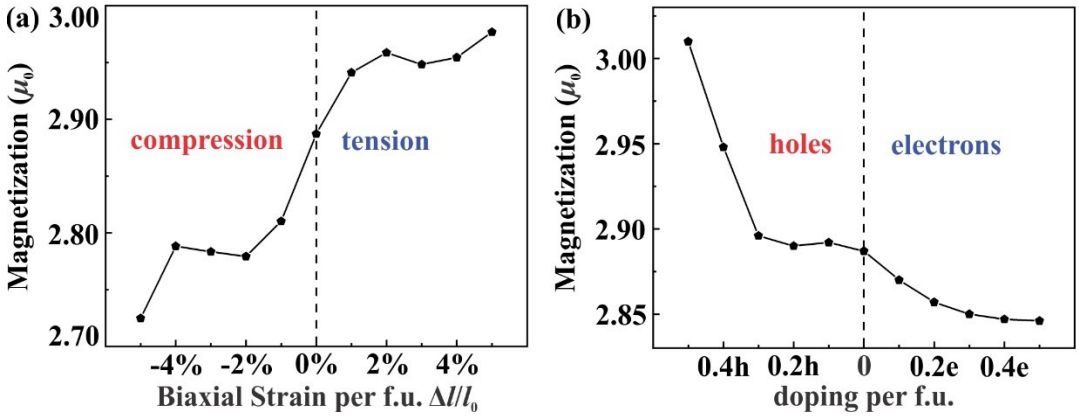

Fig. S7. The magnetic moment of Fe atom in α-FeB_3 monolayer with (a) external strain and (b) electron-hole doping, respectively.

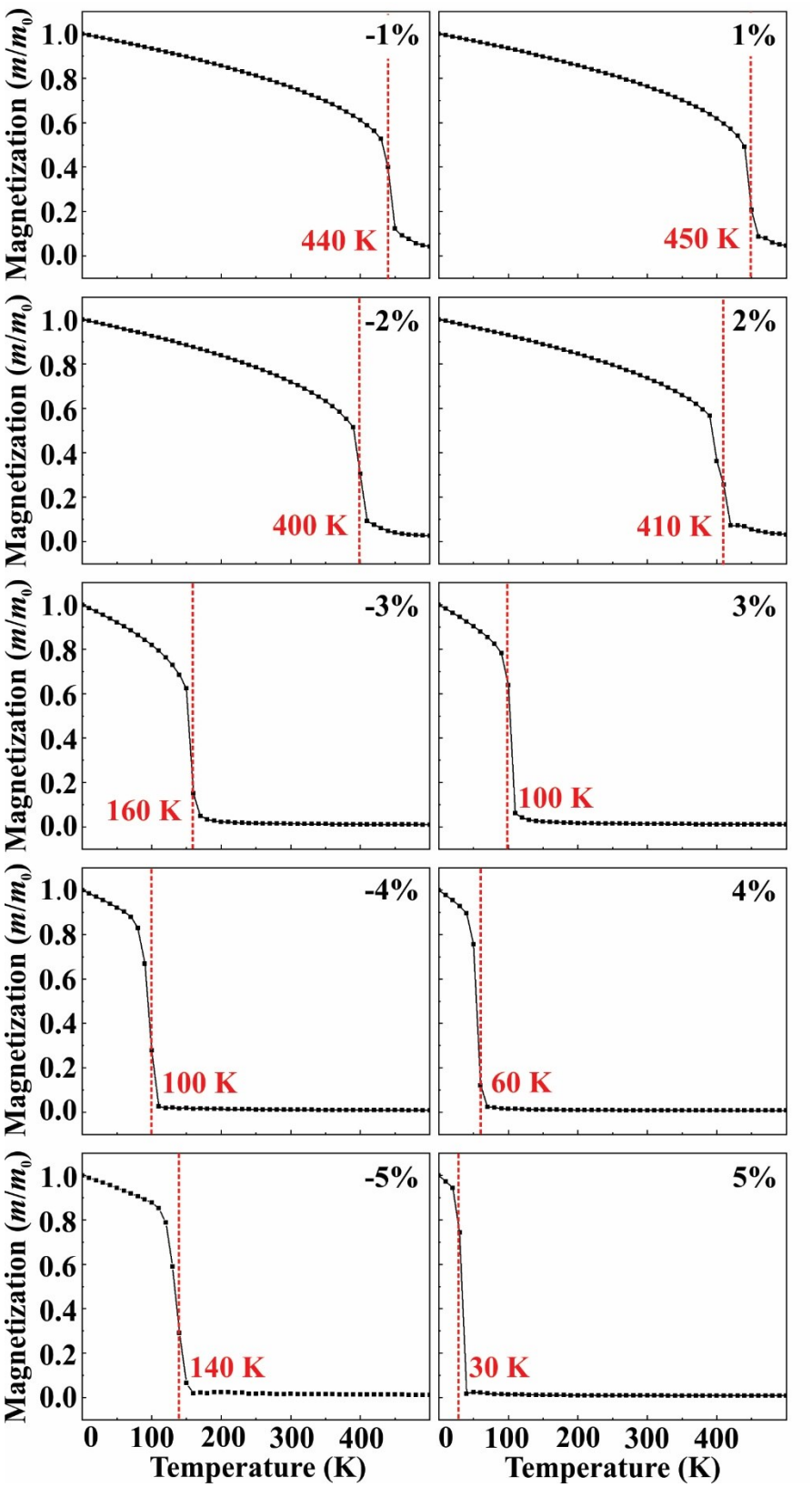

Fig. S8. The estimated Curie (Néel) temperature of α-FeB_3 monolayer under external strains by Monte Carlo simulation. The magnetic ground states of the α-FeB_3 undergoes a FM-AFM transition with the external strains over 4%.

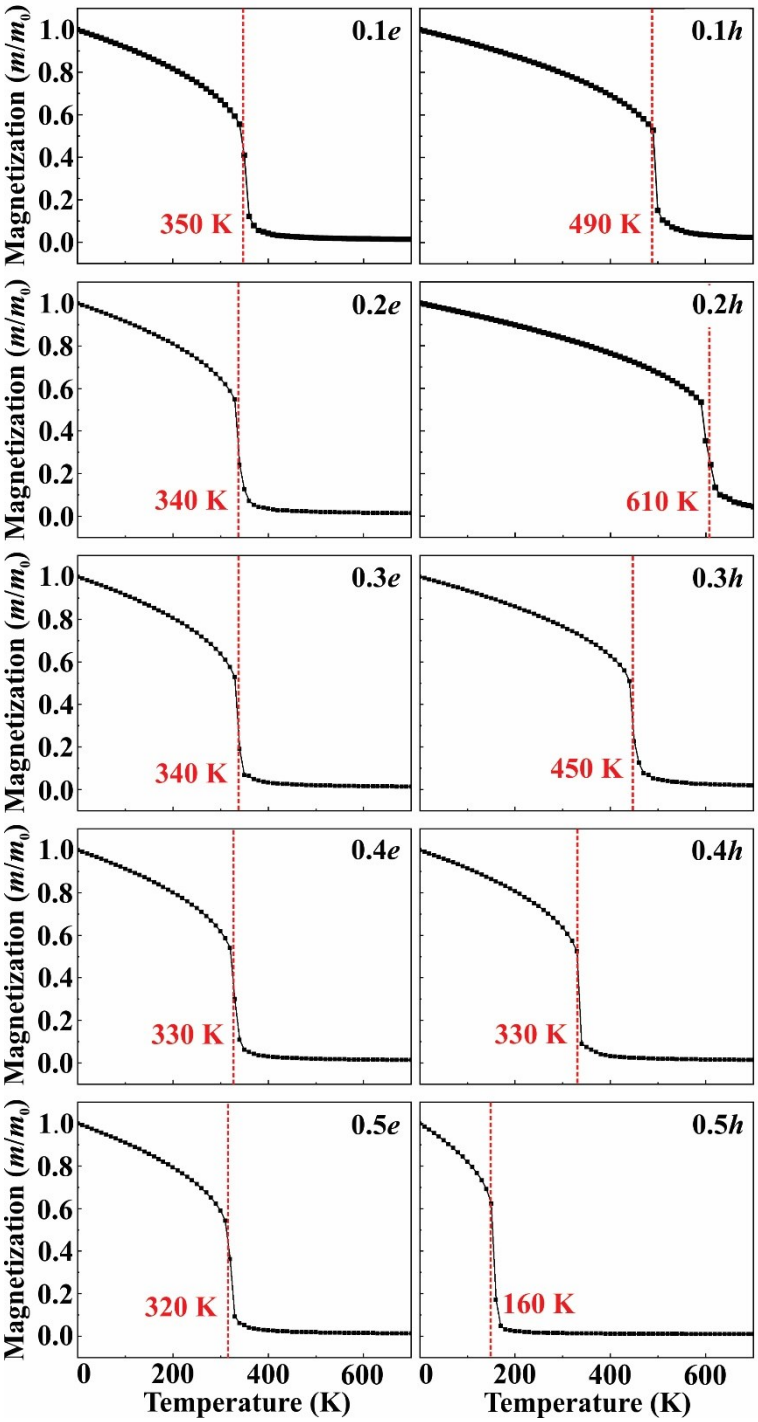

Fig. S9. The estimated Curie temperature of α-FeB_3 monolayer under charge carrier doping (0.5*h*~0.5*e*) by Monte Carlo simulation.

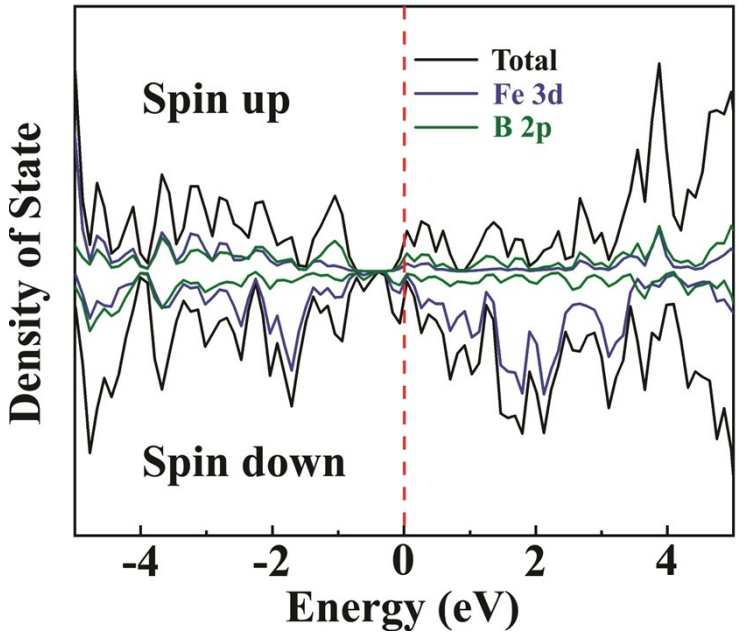

Fig. S10. Total and partial density of states of α-FeB_3 monolayer obtained by the HSE functional.

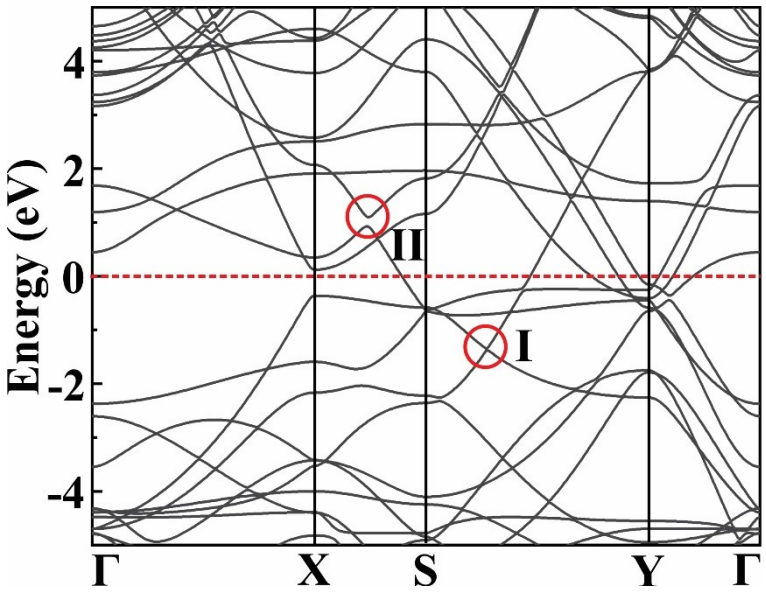

Fig. S11. The band structure of α-FeB3 monolayer by considering SOC effect.

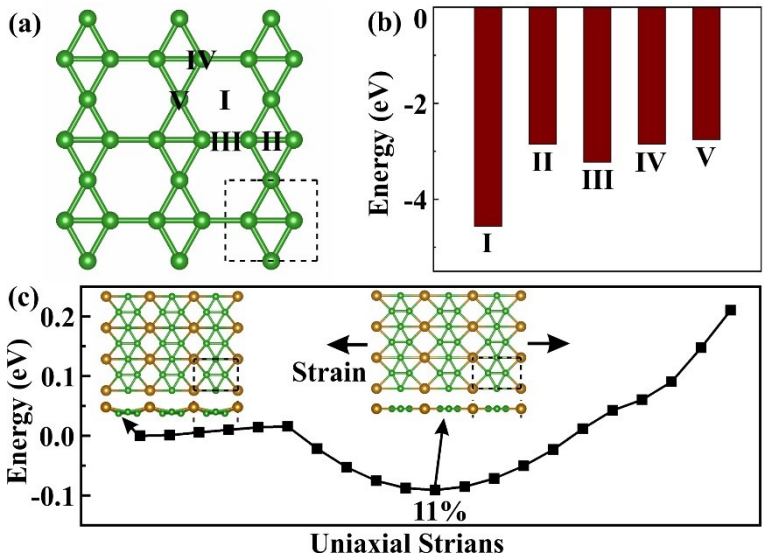

Fig. S12. (a) The geometry of δ_4 boron sheet. (b) Fe adsorption energies on the δ_4 boron sheet in different sites. (c) Total energies of optimized structures as a function of uniaxial strain. Inserts show the top and side views of Fe adsorbed boron sheet under the strain of 0% and 11%.

The planar β-FeB_3 monolayer

The β-FeB_3 possesses the total energy of 0.37 eV/atom higher than the α phase, thus, such monolayer can only be fabricated in a relatively low temperature. The β-FeB_3 monolayer (Fig. S13) shows planar hexagonal lattice with the parameter of a = 3.89 Å. In the β-FeB_3, each Fe atom is also bonded with 6 B atoms, in line with that in α-FeB_3, while B framework forms the kagome structure. It is worthy to mention that the B-B bond in the β-FeB_3 is around 1.94 Å, larger than that of boron monolayers, probably leading to the unstability in high temperature. As we can see from the ELF results, the electron gas mainly distributes in the B framework, indicating the electron transfer from Fe to B atom. Here, the Bader charge analysis shows 0.57*e* electron transfer from Fe to B framework, such value of transferred electrons is lower than that in α-FeB_3, suggesting the lower oxidation state of Fe atoms. We then calculate the cohesive energy and phonon spectrum of β-FeB_3 to briefly estimate its stability. The obtained energy is 5.77 eV/atom, suggesting its thermodynamic stability. Besides, the phonon spectrum in Fig. S13 (c) shows no imaginary frequency, indicating its kinetic stability.

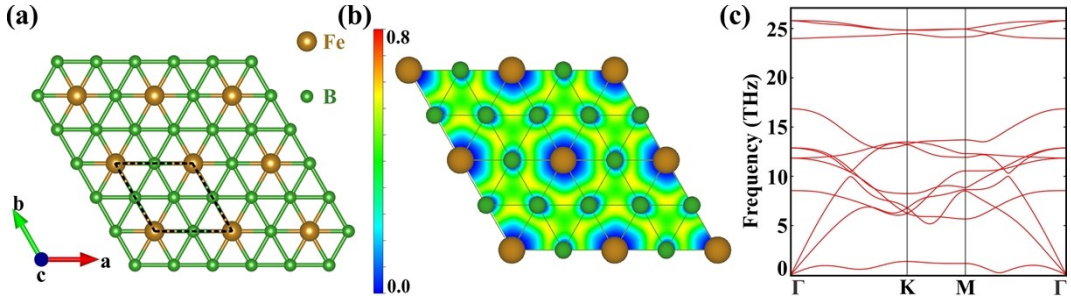

Fig. S13. (a) The geometry, (b) ELF map and (c) phonon spectrum of β-FeB_3 monolayer.

We then investigate the magnetic properties of β-FeB_3 monolayer. First, its magnetic ground state is estimated by comparing the total energies of different magnetic configurations in the 2×2 supercell (Fig. S14). The calculated energies are shown in Table S4, herein, the magnetic ground state of β-FeB_3 monolayer is AFM. In Fig. S15 (a), the spin density is mainly distributed around Fe atoms, in consistent with that in the α-FeB_3. The net magnetic moment of each Fe is 1.93 μ_B. Then, we use a square lattice to study the magnetic anisotropy for β-FeB_3. As a result, the β-FeB_3 monolayer shows out-of-plane magnetism with the value reaching 1.07 meV/Fe, which is smaller than that of α-FeB_3.

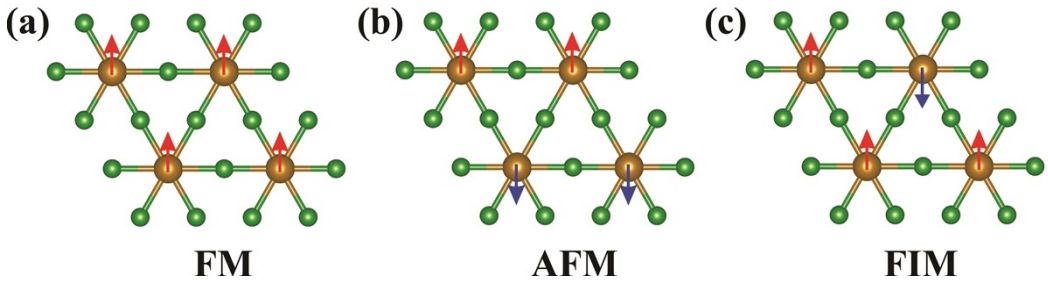

Fig. S14. The (a) FM, (b) AFM and (c) FIM configurations of the β-FeB_3 in a 2×2 supercell.

Table S4. Total energies (eV) of α-FeB_3 monolayer under different magnetic configurations. (The spin state is along the out-of-plane direction in SOC calculations.)

configurations	FM	AFM	FIM	NM
GGA+U	-91.57431	-91.85047	-91.68870	-87.96318
GGA+U+SOC	-91.64962	-91.87517	-91.70760	-

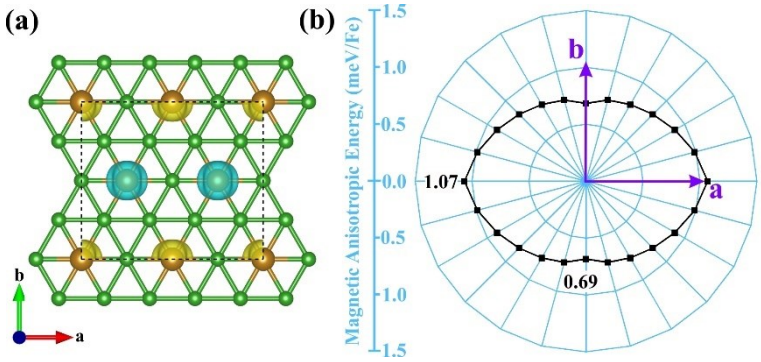

Fig. S15. (a) Spin density of β-FeB_3 monolayer. (b) The magnetic anisotropic energies in xy plane with respect to the out-of-plane direction.

Reference

1. A. Togo and I. Tanaka, *Scripta Mater.*, 2015, **108**, 1-5.
2. R. F. Evans, W. J. Fan, P. Chureemart, T. A. Ostler, M. O. Ellis and R. W. Chantrell, *J. Phys.: Condens. Matter*, 2014, **26**, 103202.
3. Y. Jiao, W. Wu, F. Ma, Z.-M. Yu, Y. Lu, X.-L. Sheng, Y. Zhang and S. A. Yang, *Nanoscale*, 2019, **11**, 16508-16514.
4. G. J. Martyna, M. L. Klein and M. Tuckerman, *J. Chem. Phys.*, 1992, **97**, 2635-2643.
5. Y. Wang, J. Lv, L. Zhu and Y. Ma, *Phys. Rev. B*, 2010, **82**, 094116.
6. Y. Wang, M. Miao, J. Lv, L. Zhu, K. Yin, H. Liu and Y. Ma, *J. Chem. Phys.*, 2012, **137**, 224108.
7. H. Zhang, Y. Li, J. Hou, A. Du and Z. Chen, *Nano Lett.*, 2016, **16**, 6124-6129.
8. H. Zhang, Y. Li, J. Hou, K. Tu and Z. Chen, *J. Am. Chem. Soc.*, 2016, **138**, 5644-5651.